Lasers in Manufacturing Conference 2019

Mass transfer by evaporation-induced gas flow at selective laser melting

A.V. Gusarov[a]*, R.S. Khmyrov[a], R.R. Ableyeva[a], T.V. Tarasova[a]

[a]*Moscow State University of Technology STANKIN, Vadkovsky per. 3a, 127055 Moscow, Russia*

Abstract

Recently observed regular motion of powder particles toward the melt pool results in formation of the denudated zones. It was supposed that the particles are transferred by the ambient gas entrained by the laser-evaporation jet. The discovered phenomenon suggests that the mass transfer in the laser-interaction zone is extremely important. In this work, the viscous gas flow is numerically modeled and the width of the denudated zone is experimentally measured. The shear stress from the gas flow is calculated at the surface of the powder layer. This stress drives powder particles. The influence of the gas parameters on the flow field and the shear stress is theoretically analyzed. The width of the denudated zone is estimated. Comparison with the experiment indicates that the balance between the drag force from the gas and the adhesion forces between powder particles determines the width of the denudated zone.

Keywords: selective laser melting; laser evaporation; denudated zone; adhesion force

1. Introduction

The so-called denudated zones are often observed at selective laser melting (SLM) of metals. They appear as thin clear bands free of powder, which separate laser-remelted bead from non-processed powder layer, and were first characterized in detail by Yadroitsev et al., 2007. According to the commonly-accepted "welding" mechanism of SLM (see, for example, Verhaeghe et al, 2009), the melt pool follows the scanning laser beam and absorbs powder particles. Such a model predicts that the remelted bead touches non-remelted powder layer without forming denudated zones. It can not explain why the melt pool attracts powder particles at the distances of several their diameters. Matthews et al., 2016, first proposed and

* Corresponding author. Tel.: +7-499-973-39-61 .
E-mail address: av.goussarov@gmail.com .

experimentally validated the gas-dynamic model for the formation of the denudated zones. According to the gas-dynamic model, an intensive evaporation jet originating at the laser spot entrains the ambient gas due to the Bernoulli effect. Near the surface of the powder layer, ambient gas flows toward the melt pool and drags powder particles. Studies of spatter formation by Gunenthiram et al., 2018, confirm the importance of gas-dynamic flow in mass transfer at SLM. Recent experiments on optical (Zhirnov et al., 2018) and X-ray (Guo et al., 2018) registration of particle dynamics in the laser-interaction zone at SLM are also consistent with the gas-dynamic model.

At laser processing, vapor flows along the external normal to the evaporating surface and can attain the sound speed (Gusarov and Smurov, 2005). At SLM, it exits from a small laser spot and is characterized by mass, momentum, and energy fluxes. Landau, 1944, showed that the most important parameter of the jet is the momentum flux (force) and obtained the exact solution of the Navier-Stokes equations for viscous fluid supposing that the force is applied in a point. This solution is referred to as the Landau submerged jet. Matthews et al., 2016, and Zhirnov et al., 2018, applied it to evaluate the entrainment flow at SLM. Zhirnov et al., 2018, showed that the experimentally measured velocities of the spatter particles outgoing from the melt pool and the powder particles incoming into the melt pool approximately correspond to the gas flow field predicted by Landau's solution. However, the Landau submerged jet can not quantitatively evaluate the entrainment gas flow at SLM because it does not take into account the non-slip boundary conditions at the surface of the powder layer. Schneider, 1981, theoretically studied viscous jet flow in a half-space and emphasized that it strongly differs from the Landau submerged jet. For example, the flow velocity in the Landau submerged jet infinitely increases with the localized force, which initiates it, while the flow velocity saturates and tends to a finite limit in a half-space jet. It particular, this explains why the width of the denudated zone does not increase with the laser power (see Zhirnov et al., 2018).

The aim of this work is to develop the model of gas-phase flow at SLM and to validate it experimentally. The drag force on a powder particle is calculated and compared with the forces of friction and adhesion. The width of the denudated zone corresponding to the calculated flowfield is estimated from the balance of forces acting on a particle. The predicted value is compared with the experimentally measured one.

2. Model

Experimental data (Zhirnov et al., 2018) as well as theory (Gusarov and Smurov, 2005) indicate that the vapor jet is always directed along the normal to the surface as shown in Fig. 1. Let axis (OZ) is the axis of the jet and plain $z = 0$ is the top surface of the processed powder layer. The problem of viscous gas flow is solved in half-space $z > 0$. It is specified by the continuity and Navier-Stokes equations, respectively,

$$\rho_t + \nabla \cdot (\rho \mathbf{u}) = 0\,, \quad (\rho \mathbf{u})_t + \nabla \cdot \mathbf{\Pi} = 0\,, \tag{1}$$

where index t indicates partial derivative with respect to time, ∇ is the Nabla operator, ρ the density, and **u** the flow velocity. The density of momentum flux is

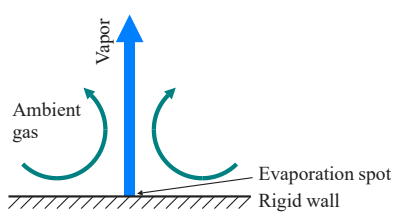

Fig. 1. Gas-phase flow at SLM

$$\mathbf{\Pi} = p\mathbf{I} + \rho\mathbf{u} \otimes \mathbf{u} - \boldsymbol{\sigma} , \tag{2}$$

where p is the pressure, $\mathbf{I}$ the unity tensor, and $\boldsymbol{\sigma}$ the viscous stress tensor,

$$\boldsymbol{\sigma} = 2\eta\left[\mathbf{e} - \frac{1}{3}\mathbf{I}\mathrm{tr}(\mathbf{e})\right], \tag{3}$$

where η is the dynamic viscosity and $\mathbf{e}$ the tensor of deformation rate defined as the symmetric part of tensor $\nabla\mathbf{u}$. The flow velocity is supposed to be small compared to the sound speed. Therefore, the gas is essentially incompressible and its density is around its density at the normal conditions ρ_0. It is also supposed that the mass of the ambient gas entrained by the vapor jet (see Fig. 1) is much greater than the mass of the vapor. Therefore, the thermal energy of vapor can be neglected and the energy equation is not considered.

Axial mass flux within circular evaporation spot with diameter D and non-slip boundary conditions outside it are specified at plane $z = 0$. Evaporation intensity increases with temperature. The temperature is equal to the boiling point and the mass flow is equal to zero at the boundary of the evaporation spot. The temperature and the mass flow attain maxima at the center of the evaporation spot. A parabolic mass flow distribution over the evaporation spot is accepted for the calculations,

$$\rho u_z = 2\rho_0 U\left(1 - \frac{4r^2}{D^2}\right), \; r \le \frac{D}{2}, \tag{4}$$

where U is the mean velocity of the vapor outflow and r the radial distance from the spot center. Equations (1) are numerically solved with boundary condition (4) by a finite-volume method with a second-order (Kurganov and Tadmor, 2000) approximation of spatial derivatives in Eq. (1).

3. Materials and experimental method

Formation of remelted beads with denudated zones is studied on 8 mm thick 12X18H10T steel substrate. The substrate is covered with 100 μm thick powder layer and scanned by a laser beam with parameters listed in Table 1. Two WC-Co powders are tested: fine powder WOKA 3660 FC with mean particle size 25 μm shown in Fig. 2a and coarse powder WOKA 3110 with mean particle size 50 μm shown in Fig. 2b. Top views of the laser-processed samples with single remelted beads are observed by optical microscope. The particles of non-melted particles are fixed on the substrate with hot melt glue. Seven cross-sections of each sample are studied by a standard metallography with optical microscope. The cross-sections are prepared by consecutive grinding with the step of 0.5 mm. The effective width of the denudated zone is evaluated in each cross-section from the profile of particle distribution. The mean and the standard deviation are calculated.

Table 1. Parameters of the laser processing

Parameter	Wavelength	Spot diameter	Beam power	Scanning speed
Value	1064 nm	100 μm	170 W	50 mm/s

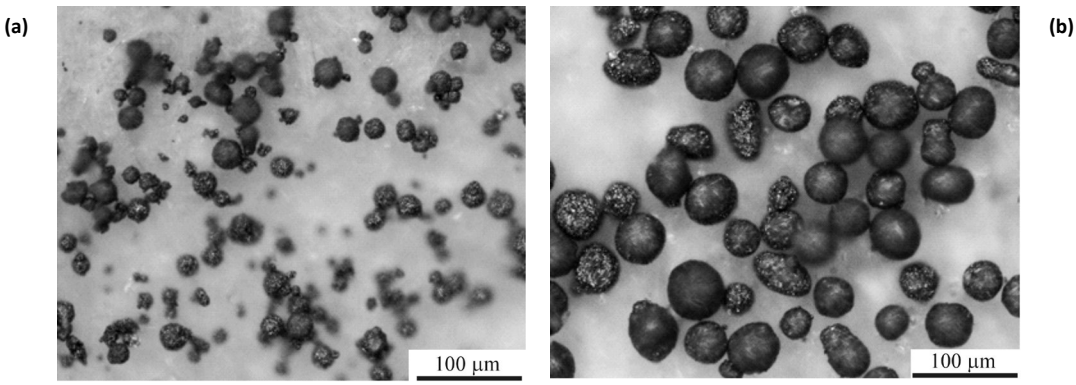

Fig. 2. Fine (a) and coarse (b) WC-Co powders

4. Results

Calculations are made for Ar atmosphere at the atmospheric pressure and the temperature 298 K. The gas parameters accepted for the calculations are listed in Table 2. The diameter of the evaporation spot is accepted to be $D = 50$ μm. The intensity of evaporation is specified by the Reynolds number at the evaporation spot

$$\mathrm{Re} = \frac{DU}{\nu}, \tag{5}$$

where ν is the cinematic viscosity. Figure 3 shows the examples of the calculated gas-dynamic fields. The velocity fields are compared with flowlines of the corresponding Landau submerged jet (see dashed lines in the left column of Fig. 3). The calculated velocity field approximates the Landau field in the near-axis domain but considerably deviates from it near the boundary plane because of the different boundary conditions. One can also see from Fig. 3 that the gas velocity increases and the angle of divergence of the entrainment flow decreases with increasing Re. Near the surface (plane $z = 0$), gas flows toward the center. Figure 4 shows the shear stress on the surface calculated from the gas-dynamic fields. The shear stress decreases with the distance from the center approximately as $1/r^3$ at $\mathrm{Re} = 10$ and as $1/r^2$ at $\mathrm{Re} = 20$ and 30 (see dashed lines in Fig. 4).

Table 2. Properties of Ar ambient gas

Parameter	Density, ρ_0	Dynamic viscosity, η	Cinematic viscosity, ν
Value	1.634 kg/m^3	$22.3 \cdot 10^{-6}$ Pa s	$13.65 \cdot 10^{-6}$ m^2/s

Figure 5 shows top views of the laser-processed samples where remelted beads and denudated zones are clearly seen. In the case of fine 25 μm powder (see Fig. 5a), the external boundary of the denudated zone is well-defined but extremely waved. In the case of coarse 50 μm powder (see Fig. 5b), the external boundary is diffuse and separated powder particles are observed inside the denudated zone. This is why multiple cross-sections of each sample are studied. Figure 6 shows the examples of cross-section. Table 3 lists the results of the statistical analysis of the cross-sections. Here, the width of the denudated zone L is the

distance from its left external boundary to the right external boundary across the remelted bead. The results clearly indicate that the width of the denudated zone increases with the powder particle size.

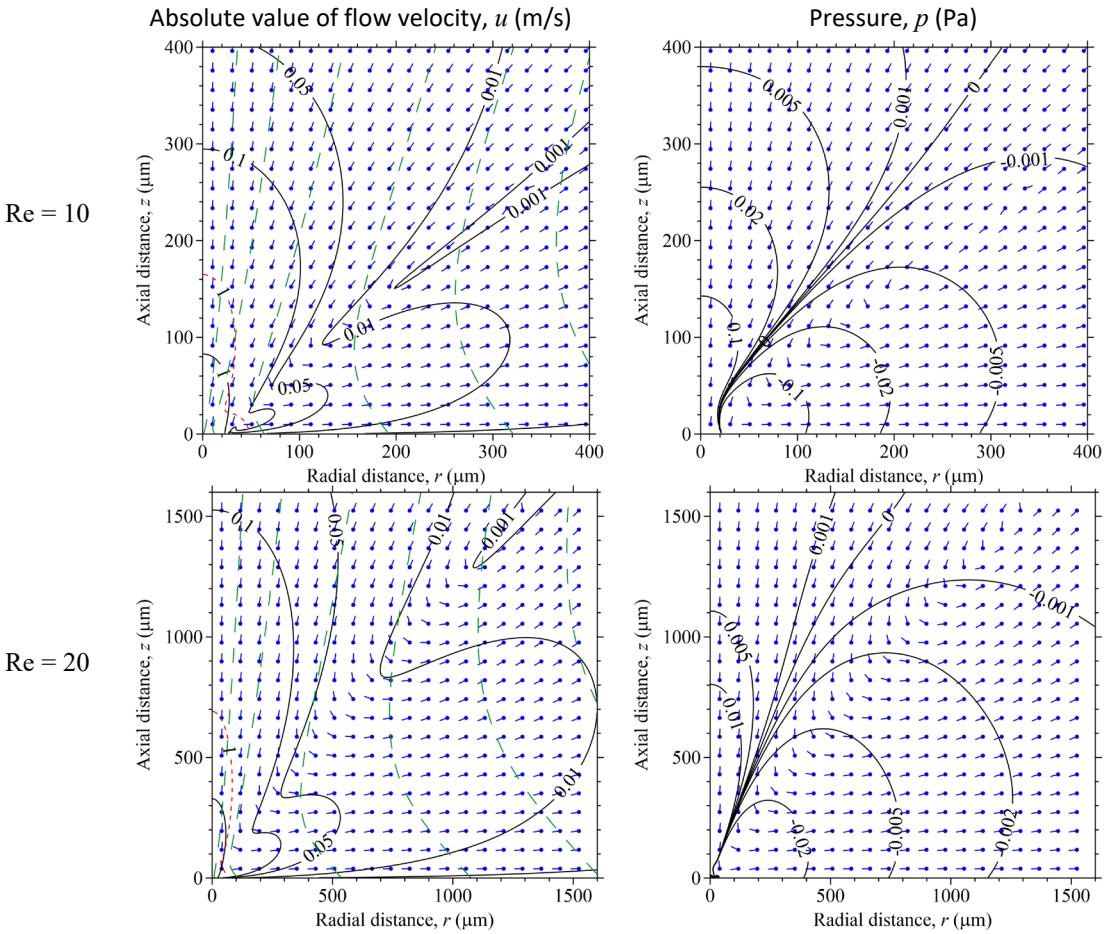

Fig. 3. Calculated fields (full contour lines) of the absolute value of velocity (left column) and pressure (right column) at two values of the Reynolds number: Re = 10 (upper row) and Re = 20 (lower row). Flags indicate the direction of the velocity vector. Dashed lines are flowlines of the Landau submerged jet

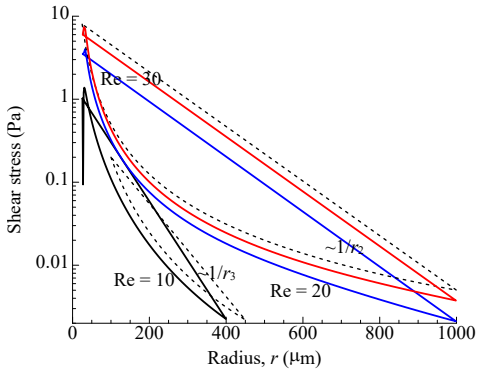

Fig. 4. Calculated shear stress on the surface

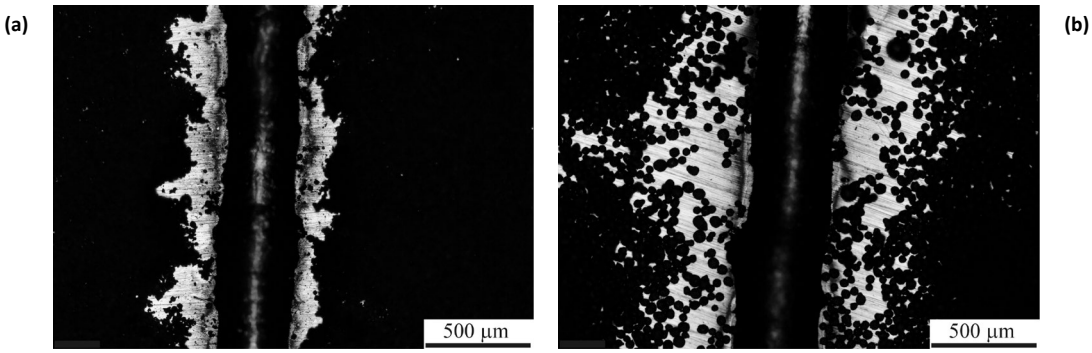

Fig. 5. Top view of remelted beads with denudated zones: fine (a) and coarse (b) WC-Co powders

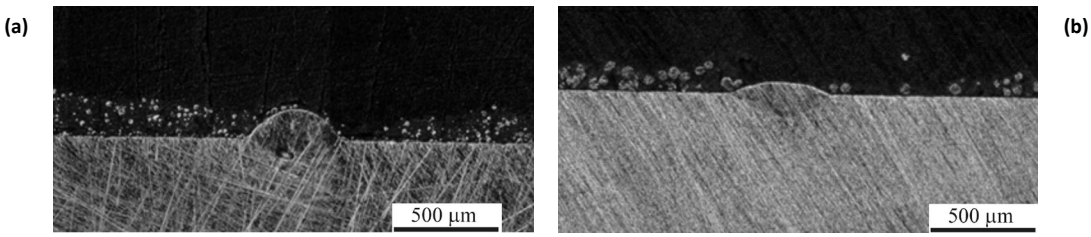

Fig. 6. Cross sections of remelted beads with denudated zones: fine (a) and coarse (b) WC-Co powders

Table 3. Experimentally measured width of the denudated zone, L

Parameter	Mean particle diameter	L	Standard deviation of L
Fine powder	25 μm	640 μm	90 μm
Coarse powder	50 μm	890 μm	160 μm

5. Discussion

The calculations of gas flow in the laser-interaction zone at SLM indicate that a drag force acts on the surface of the powder layer, which tends to move powder particles toward the evaporation spot. Figure 4 shows the calculated shear stress distribution. The drag force applied to a particle on the top of the particle layer is estimated as the shear stress σ multiplied by the projection area of the particle $\pi d^2/4$, where d is the particle diameter,

$$F_d = \sigma \pi d^2/4 , \quad (6)$$

The drag force decreases with the distance from the center along with the shear stress. The forces of friction F_f and adhesion F_a applied to a particle from its neighbors resist the drag force. Finally, the force balance determines the width of the denudated zone. The friction force is proportional to particle mass, $\pi \rho d^3/6$,

$$F_f = \mu \pi \rho g d^3/6 , \quad (7)$$

where ρ is the density of particle material, μ the friction coefficient, and g the gravity acceleration. The adhesion Van-der-Waals force between two spheres of diameter d is (Meier et al., 2019)

$$F_a = \frac{Ad}{24\varepsilon^2} , \quad (8)$$

where A is the Hamaker constant and ε the gap distance between particles. Note the quite different dependences of the forces on particle diameter d: the adhesion force is proportional to d, the drag force is proportional to d^2, and the friction force is proportional to d^3.

First, suppose that the friction force is much greater than the adhesion force. Then from balance $F_d = F_f$, one can obtain

$$\sigma = \frac{2}{3} \mu \rho g d . \quad (9)$$

Remember that shear stress σ is a decreasing function of radial distance r (see Fig. 4). The solution of Eq. (9) relative r is the half-width of the denudated zone $L/2$. The right hand side of Eq. (9) is an increasing function of particle diameter d. Therefore, L is a decreasing function of d. This contradicts to the experimental result that L increases with d (see Table 3). In the opposite case when the friction force is much less than the adhesion force, balance $F_d = F_a$ results

$$\sigma = \frac{A}{6\pi d \varepsilon^2} . \quad (10)$$

The right hand side of Eq. (10) is a decreasing function of particle diameter d. Therefore, L is an increasing function of d. This agrees with the present experimental data.

The above theoretical interpretation of the experimental data indicates that the adhesion forces between powder particles are more important than the friction ones in the considered conditions of SLM. The same conclusion was made by Meier et al., 2019 from their studies of particle dynamics.

Conclusions

A mathematical model is developed to calculate the entrainment flow of ambient gas induced by evaporation at SLM. The calculations indicate that the flow velocity increases and the divergence angle of the entrainment flow decreases with the intensity of evaporation. Near the powder layer surface, gas flows toward the evaporation spot and leads to shear stress applied to the surface, which tends to drag powder particles. The calculated shear stress distribution allowed to estimate the denudated zone width from the balance of the drag, friction, and adhesion forces.

An experimental method is proposed to fix the particles of free-poured powder to study the denudated zone at SLM. Experiments with 25 μm and 50 μm WC-Co powders indicate that the denudated zones can have strongly waved or diffuse boundaries. However, statistical analysis of multiple cross-sections gives the effective width of the denudated zone. The width of the denudated zone is shown to increase with the particle diameter.

Comparison of the experimental and the theoretical results indicates that the adhesion forces between powder particles are more important than the friction ones at the considered conditions of SLM.

Acknowledgements

This work is supported by Russian Science Foundation (Grant Agreement No. 15-19-00254).

References

Gunenthiram, V., Peyre, P., Schneider, M., Dal, M., Coste, F., Koutiri, I., Fabbro, R., 2018. Experimental analysis of spatter generation and melt-pool behavior during the powder bed laser beam melting process. J. Mater. Process. Techn. 251, p. 376.

Guo, Q., Zhao, C., Escano, L.I., Young, Z., Xiong, L., Fezzaa, K., Everhart, W., Brown, B., Sun, T., Chen, L.., 2018. Transient dynamics of powder spattering in laser powder bed fusion additive manufacturing process revealed by in-situ high-speed high-energy x-ray imaging. Acta Mater. 151, p. 169.

Gusarov, A.V., Smurov, I., 2005. Thermal model of nanosecond pulsed laser ablation: Analysis of energy and mass transfer. J. Appl. Phys. 97, p. 014307.

Kurganov, A., Tadmor, E., 2000. New high-resolution central schemes for nonlinear conservation laws and convection-diffusion equations. J. Computat. Phys. 160, p. 241.

Landau, L., 1944. A new exact solution of the Navier-Stokes equations. Doklady Akademii Nauk SSSR, 43, p. 299.

Matthews, M.J., Guss, G., Khairallah, S.A., Rubenchik, A., Anderson, A.T., Depond, P.J., King, W.E., 2016. Denudation of metal powder layers in laser powder bed fusion processes. Acta Mater. 114, p. 33.

Meier, C., Weissbach, R., Weinberg, J., Wall, W.A., Hart, A.J., 2019. Critical influences of particle size and adhesion on the powder layer uniformity in metal additive manufacturing. J. Materials Processing Techn. 266, p. 484.

Schneider, W., 1981. Flow induced by jets and plumes. J. Fluid Mech. 108, p. 55.

Verhaeghe, F., Craeghs, T., Heulens, J., Pandelaers, L., 2009. A pragmatic model for selective laser melting with evaporation. Acta Mater. 57, p. 6006.

Yadroitsev, I., Bertrand, Ph., Smurov, I., 2007. Parametric analysis of the selective laser melting process. Appl. Surf. Sci., 253, p. 8064.

Zhirnov, I., Kotoban, D.V., Gusarov, A.V., 2018. Evaporation-induced gas-phase flows at selective laser melting. Appl. Phys.A 124, p. 157.